energy&fuels

Article

pubs.acs.org/EF

Extraction of Hydrocarbons from High-Maturity Marcellus Shale Using Supercritical Carbon Dioxide

Palma J. Jarboe,*[,†,⊥] Philip A. Candela,[‡] Wenlu Zhu,[‡] and Alan J. Kaufman[‡,§]

[†]U.S. Geological Survey, Reston, Virginia 20192, United States

[‡]Department of Geology, University of Maryland, College Park, Maryland 20742, United States

[§]Earth System Science Interdisciplinary Center, University of Maryland, College Park, Maryland 20742, United States

ABSTRACT: Shale is now commonly exploited as a hydrocarbon resource. Due to the high degree of geochemical and petrophysical heterogeneity both between shale reservoirs and within a single reservoir, there is a growing need to find more efficient methods of extracting petroleum compounds (crude oil, natural gas, bitumen) from potential source rocks. In this study, supercritical carbon dioxide (CO_2) was used to extract *n*-aliphatic hydrocarbons from ground samples of Marcellus shale. Samples were collected from vertically drilled wells in central and western Pennsylvania, USA, with total organic carbon (TOC) content ranging from 1.5 to 6.2 wt %. Extraction temperature and pressure conditions (80 °C and 21.7 MPa, respectively) were chosen to represent approximate *in situ* reservoir conditions at sample depth (1920−2280 m). Hydrocarbon yield was evaluated as a function of sample matrix particle size (sieve size) over the following size ranges: 1000−500 μm, 250−125 μm, and 63−25 μm. Several methods of shale characterization including Rock-Eval II pyrolysis, organic petrography, Brunauer−Emmett−Teller surface area, and X-ray diffraction analyses were also performed to better understand potential controls on extraction yields. Despite high sample thermal maturity, results show that supercritical CO_2 can liberate diesel-range (*n*-C_{11} through *n*-C_{21}) *n*-aliphatic hydrocarbons. The total quantity of extracted, resolvable *n*-aliphatic hydrocarbons ranges from approximately 0.3 to 12 mg of hydrocarbon per gram of TOC. Sieve size does have an effect on extraction yield, with highest recovery from the 250−125 μm size fraction. However, the significance of this effect is limited, likely due to the low size ranges of the extracted shale particles. Additional trends in hydrocarbon yield are observed among all samples, regardless of sieve size: 1) yield increases as a function of specific surface area (r^2 = 0.78); and 2) both yield and surface area increase with increasing TOC content (r^2 = 0.97 and 0.86, respectively). Given that supercritical CO_2 is able to mobilize residual organic matter present in overmature shales, this study contributes to a better understanding of the extent and potential factors affecting the extraction process.

INTRODUCTION

Hydraulic fracturing has proven to be a successful well stimulation technique, enhancing matrix permeability of unconventional reservoirs and thus, improving production of oil and natural gas.[1,2] However, due to variability in both organic and inorganic components found among different shale formations and within a single reservoir, there remains a need to develop different fracturing fluid systems that can optimize well productivity.[2] In this regard, carbon dioxide (CO_2) may provide an extraction alternative to conventional water-based fluids in both water-sensitive (i.e., those with an abundance of expanding clay minerals) and oil-wet formations that preferentially imbibe oil.[2−4] Consequently, the potential use of CO_2 as a non-aqueous working fluid in hydraulic fracturing and unconventional oil and gas (UOG) development is currently being investigated.[2,4−11]

Supercritical fluid extractions use high-density gases to extract a variety of organic compounds from solid matrices. Higher, liquid-like solvent densities observed in the supercritical region enhance solvent strength or dissolving power, enabling the supercritical fluid to vaporize some higher molecular weight, low volatility compounds at temperatures below their normal boiling points.[12,13] However, by virtue of the gaseous properties of the solvent, supercritical fluids maintain higher diffusivity, lower viscosity, and lower surface tension compared to conventional liquid solvents, improving mass transfer through the sample matrix and increasing extraction rates.[13−16] Carbon dioxide exists in a supercritical state at temperatures and pressures greater than its critical point of 30.978 ± 0.015 °C (critical temperature, T_c) and 7.3773 ± 0.0030 MPa (critical pressure, P_c).[17] At this critical point, CO_2 has a critical density of 467.6 ± 0.6 kg/m^3.[17]

Supercritical CO_2 has successfully extracted and separated a wide range of non-polar aliphatic and polycyclic aromatic hydrocarbons from shale and coal under varying extraction parameters.[13−15,18−21] The effective molecular diameter of CO_2, 3.3 Å,[22] enables CO_2 to access micropores of coal and shale matrices.[22−26] Monin et al.[14] extracted *n*-aliphatic hydrocarbons from diverse shale source rocks (of the Mahakam Delta, Indonesia, the Douala Basin, Cameroon, and the Paris Basin, France) in the range of *n*-C_{10} through *n*-C_{34} with supercritical CO_2 (at 40 °C and 20 MPa). Li et al.[15] extracted similar ranges of aliphatic and aromatic hydrocarbons from U.S. shales and coals of the Fruitland and Pottsville Formations (Cretaceous and Pennsylvanian periods, respectively) at 120 °C and 20.3 MPa, but focused on quantifying the recovery of more volatile (C_6 to C_{14}) hydrocarbons, with yields ranging between 0.01 and 0.2 wt % (grams of extracted hydrocarbon per gram of

Received: September 11, 2015
Revised: October 30, 2015
Published: November 2, 2015

DOI: 10.1021/acs.energyfuels.5b02059
Energy Fuels 2015, 29, 7897−7909

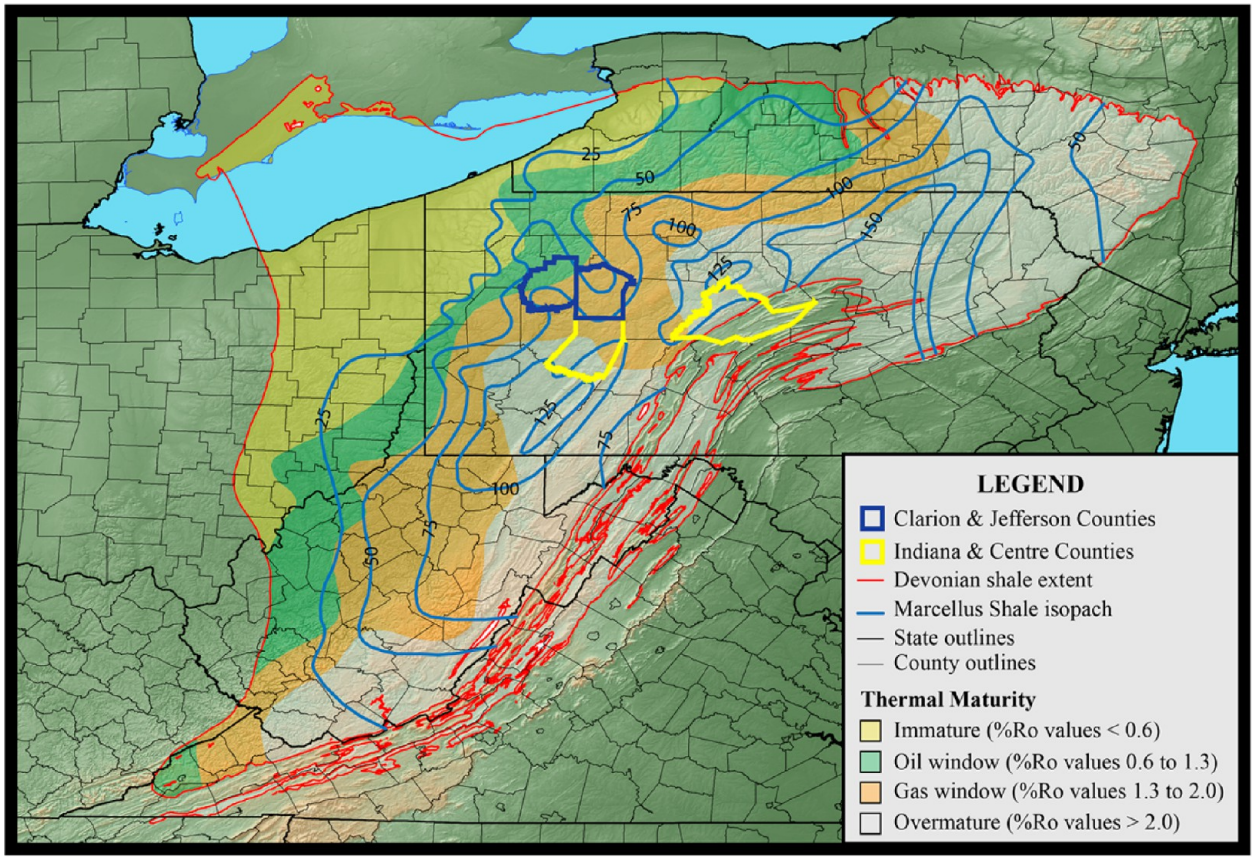

Figure 1. Map of the Marcellus Shale, with thermal maturity zones, isopach lines,[43] and sampled Pennsylvania counties. Map modified from East et al.[44] Samples from the 3S (Clarion County), 2LT and 4LG (Jefferson County), and 2LK (Centre County) cores were donated courtesy of EXCO Resources, Inc. Samples from the EG (Indiana County) core were donated courtesy of the Pennsylvania Geological Survey, Department of Conservation and Natural Resources.

sample). However, both studies normalized their yields to the sample mass, with no report of organic richness, type, thermal maturity, or mineralogy. Consideration of organic and inorganic shale matrices is important in assessing extraction potential as these compositional elements directly impact pore structure and connectivity, hydrocarbon sorption capacities, and transport processes within shale reservoirs.[27−30]

Normalizing oil content or extractable organic matter (EOM) to total organic carbon (TOC) content thus provides a more accurate indication of production potential relative to absolute yields.[31] Furthermore, sorption capacities of both oil and gas are also known to increase with TOC, as does micro- and nanoscale porosity (volume and surface area) within organic matter, in thermally mature shales.[27−29,31] Results of this study have thus been normalized to TOC to better evaluate extracted hydrocarbon yield relative to the organic matter present within the shale samples. Given the heterogeneous geochemical and geophysical characteristics of shale reservoirs, this will hopefully also provide a better means of comparing extraction yields from shales across different maturity levels in future extraction studies.

Supercritical CO_2 extraction studies have assessed the effect of sample particle size distribution (from approximately 0.07 mm to 2.0 mm in diameter) on extraction efficiency from various solid matrices (oil shale, paprika, cocoa nibs).[32−34] All show an increase in recovery of organic compounds with decrease in sieve size. Authors of these studies attribute this trend to an increase in exposed sample surface area associated with smaller particles, which enhances accessibility of the solvent to the extractable compounds, creates shorter diffusion paths, enhances mass transfer through the sample matrix, and thus ultimately increases overall extraction rates. However, other authors[35,36] have suggested that there may be an optimum particle size (sieve size) in supercritical fluid extractions, ranging from approximately 2.0 mm to 250 μm. If particle sizes are too small, channeling of solvent flow can occur within the extraction cell. These directed flow paths can reduce interactions between the solvent and extractable compounds, resulting in a decline in extraction efficiency and overall recovery.[35,36] Lower extraction efficiencies sometimes encountered with sieve sizes below this range have also been associated with particle aggregation,[37] and with higher capillary entry pressures, which can require greater force to extract hydrocarbons from porous media.[38] The process of grinding samples into smaller particles may change grain size distributions based on mineral hardness, and also lead to loss of volatile compounds,[35] both of which may affect extraction yields.

Consequently, a deeper investigation into the effect of shale matrix particle size on hydrocarbon recovery in supercritical fluid extractions is needed to better understand the mechanisms of CO_2−hydrocarbon interactions within shale matrices. This study seeks to contribute to a better understanding of the extent and controls on the mobilization process, which is important if CO_2 is to be used as a working fluid for hydraulic fracturing and UOG development.[2,5−11] Understanding these

DOI: 10.1021/acs.energyfuels.5b02059
Energy Fuels 2015, 29, 7897−7909

Table 1. Rock-Eval II Pyrolysis Results for Selected Core Samples for Supercritical CO_2 Extractions

			resource potential				type of organic matter			thermal maturation	
core-sample ID[a]	county, PA	vertical depth (m)	TOC[b]	S1[c]	S2[c]	S1/TOC[d]	S3[e]	HI[f]	OI[g]	PI	T_{max}[h]
3S-8	Clarion	1924	4.8	2.8	0.7	58.8	0.4	14.6	7.9	0.8	517
3S-29	Clarion	1951	6.2	0.7	0.7	11.8	0.3	11.5	5.2	0.5	547
2LT-12	Jefferson	2267	3.2	0.8	0.5	24.3	0.2	16.4	6.3	0.6	364
2LT-19	Jefferson	2277	3.7	0.7	0.6	19.0	0.3	16.0	8.4	0.5	380
4LG-3	Jefferson	2008	3.9	0.9	0.4	23.8	0.3	9.6	7.5	0.7	359
4LG-18	Jefferson	2025	1.5	1.0	0.3	64.5	0.6	17.1	38.2	0.8	341
4LG-25	Jefferson	2031	5.6	1.2	0.4	20.9	0.2	7.5	3.0	0.7	533

[a]Samples courtesy of EXCO Resources, Inc. [b]TOC (wt %). [c]S1 and S2 (mg HC/g rock). [d]S1/TOC (mg HC/g TOC). [e]S3 (mg CO_2/g rock). [f]HI (mg HC/g TOC). [g]OI (mg CO_2/g TOC). [h]T_{max} (°C).

interactions is also important in terms of caprock integrity at geologic CO_2 storage sites. Injection of CO_2 has the potential to react with the caprock, potentially altering matrix porosity and permeability, and increasing levels of dissolved organic carbon and alkalinity within *in situ* brines.[39−42]

The primary objective of this study is to determine the quantity and distribution of *n*-aliphatic hydrocarbons that can be extracted from Marcellus Shale samples with supercritical CO_2 as a function of sample matrix particle size (sieve size), at estimated *in situ* pressure and temperature conditions. Selected particle size ranges (1000−500 μm, 250−125 μm, and 63−25 μm) include two ranges below the optimum range suggested above.[35,36] Results are evaluated as a function of the following: (1) Rock-Eval II pyrolysis and TOC analysis to evaluate source rock potential (quantity, quality and thermal maturity of organic matter); (2) reflectance analysis to determine thermal maturity and identify organic matter type; (3) X-ray diffraction (XRD) to determine mineral abundances; (4) Brunauer−Emmett−Teller (BET) surface area analysis of the selected sieve sizes; and (5) scanning electron microscopy (SEM) imaging to visualize shale surface and porosity characteristics.

EXPERIMENTAL SECTION

Sampling. Cores intersecting the Marcellus Shale were donated from EXCO Resources, Inc., and the Pennsylvania Geological Survey, Department of Conservation and Natural Resources. All samples are from vertically drilled wells located in central and western Pennsylvania, with subsurface depths ranging from approximately 1920 m to 2280 m (Figure 1). Exact well locations and drilling fluid compositions are unknown. Specimens from different sedimentary facies throughout the five cores were sampled for potential use in the supercritical CO_2 extraction experiments.

Rock-Eval II Pyrolysis and Total Organic Carbon Analysis. Samples were sent to GeoMark Research, Ltd. for Rock-Eval II pyrolysis and TOC analysis to provide an initial screening of shale source rock potential. Pyrolysis was performed on a Rock-Eval II instrument, and TOC analysis on a LECO C230 instrument. Rock-Eval II measured parameters include (1) the S1 peak, representing free, thermally extractable hydrocarbons present in the rock, expressed in units of milligrams of hydrocarbon (HC) per gram of rock; (2) the S2 peak, representing the abundance of hydrocarbons generated from pyrolytic cracking of the remaining kerogen, expressed in units of milligrams of HC per gram of rock; (3) T_{max} (°C), which is the temperature recorded at the maximum generation of hydrocarbons within the S2 peak; and (4) the S3 peak, representing CO_2 content, expressed in units of milligrams of organic CO_2 per gram of rock.[45,46] Based on results, seven samples (from the 3S, 2LT, and 4LG cores) were selected for further geochemical characterization and subsequent supercritical CO_2 extractions (Table 1). Chosen samples were considered to have the greatest extraction potential, with selection criteria based on the highest S1 (>0.70 mg HC/g rock) and S1/TOC (mg HC/g TOC) values. The S1/TOC value, also referred to as the oil saturation index, normalizes oil content to TOC and is used as an indicator of *in situ* source rock potential.[31]

Sample Preparation. Each sample was crushed to a powder with a stainless steel mortar and pestle. Crushed samples were subsequently dry-sieved by using a nested stack of U.S.A. Standard sieves into the following size fractions: 1000−500 μm (18−35 mesh), 250−125 μm (60−120 mesh), and 63−25 μm (230−500 mesh). The 1000−500 μm and 250−125 μm size fractions were chosen to represent coarse and fine sand-size grains, respectively, and the 63−25 μm fraction was chosen to represent silt-size grains. Sample splits of each sieve size were then taken following the cone-and-quartering homogenization technique.[47] Sample splits were reserved for the supercritical CO_2 extractions and the following shale geochemical characterization analyses: (1) reflectance; (2) XRD; (3) BET surface area; and (4) SEM imaging. All size fractions and samples splits were stored in glass jars that were previously baked in a high-temperature muffle furnace (at 450 °C for 6 h) and sealed with polytetrafluoroethylene (Teflon)-lined lids until ready for analysis.

Reflectance Analysis. Reflectance analysis, performed in accordance with ASTM D7708[48] at the Organic Petrology Laboratory at the U.S. Geological Survey (USGS) in Reston, Virginia, was used to confirm the thermal maturity of the samples and to potentially identify the type of organic matter present. One sample from each core (3S-8, 2LT-12, and 4LG-3) was analyzed given the minor depth interval (<27 m) between samples within each core. Prior to analysis, the ground samples were mounted in a heat-setting thermoplastic to create pellets in a Buehler Simplimet 3000 Automatic Mounting Press, and subsequently polished with a Buehler Ecomet 4 according to ASTM D2797.[49] Reflectance measurements were made on a Leica DMRX incident light microscope equipped with a tungsten halogen discharge light source and a photomultiplier detector. Results were recorded as the percentage of incident white light reflected from the sample, $\%R_o$. Measurements were taken by using an oil immersion objective lens to increase microscope resolution, and calibrated against a glass standard (1.314 $\%R_o$). Average values were reported based on a total of 21−24 measurements for each sample with reported uncertainties within ±0.5 $\%R_o$. Quality assurance/quality control (QA/QC) was performed on a Hilgers microscope system with LED light source and digital camera detector.

X-ray Diffraction. XRD was performed at the USGS in Reston, Virginia, to identify and quantify mineral constituents present within the samples. Prior to analysis, powdered shale samples (63−25 μm) were dried at 100 °C and then ashed at <100 °C.[50] Ashed samples were mounted as 25 mm pellets. XRD analyses were performed on a PANalytical X'Pert PRO X-ray diffractometer, where the sample pellets were irradiated with monochromatic Cu Kα X-radiation. Mineral phase identification and abundances were achieved by comparing the sample XRD patterns against a library of reference mineral standards.[51,52] Absolute uncertainties for measured mineral abundances are within ±1% (1σ).

Supercritical Fluid Extractions. Hydrocarbon extractions of all samples were performed on an ISCO SFX 220 supercritical fluid

DOI: 10.1021/acs.energyfuels.5b02059
Energy Fuels 2015, 29, 7897−7909

extraction system coupled with an ISCO 260D model syringe pump at a USGS laboratory in Reston, Virginia. Borehole temperature data were not available for the shale samples used in this study, and thus, temperature and pressure conditions, 80 °C and 20.7 MPa (3000 psi), respectively, were chosen to represent approximate *in situ* reservoir conditions at sample depth (1920−2280 m), based upon a geothermal gradient of 30 °C/km (with an average surface temperature of 20 °C) and subsurface pressure gradient of 10.5 MPa/km (0.465 psi/ft).[53] At 80 °C and 20.7 MPa (3000 psi), the density of CO_2 is approximately 600 kg/m^3.[54,55]

Extraction protocols were adapted from USGS Open-File Report 2006-1054.[56] Each extraction consisted of a 15 min static step, followed by a 1 hr dynamic step, with a corresponding flow rate of approximately 1.0−1.5 mL/min, whereby the total volume of CO_2 dispensed ranged between approximately 70 and 90 mL. A high restrictor (outlet line) temperature of 100 °C was chosen to minimize precipitation of heavy hydrocarbons or ice that could plug the line and reduce hydrocarbon recovery.[14,15] Temperature settings on the extractor were controlled by a Fuji electric sensor with a manufacturer accuracy of ±1 °C. The temperature sensor was calibrated using an alcohol thermometer, and the expected accuracy was confirmed. Pressure was also digitally controlled by the extractor, but was calibrated using an external NIST-certified pressure gauge (McMaster-Carr) to within a reported accuracy of ±3% (±0.69 MPa, 100 psi) of the target pressure (20.7 MPa, 3000 psi).

The extraction cell consisted of a 10 mL aluminum vessel with 2 μm opening frit filters inserted beneath the top and bottom vessel lids (Figure 2). A 1.0 g ground sample was added to the vessel, sandwiched between two small layers of quartz wool to minimize dead volume. The amount of O_2 in an empty vessel was estimated to be 2.1 mL. During extractions the vessel was approximately 90% filled with the sample and quartz wool; thus the O_2 content decreased by approximately 1 order of magnitude (2% of total cell volume).

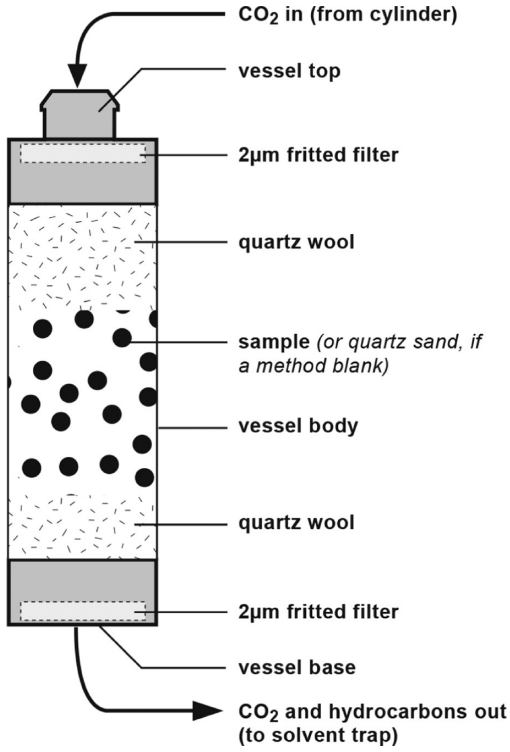

Figure 2. Aluminum vessel used in supercritical CO_2 extractions (10 mL capacity). Not drawn to scale. Modified from Kolak.[56]

Extracts were collected in 100 mL of chilled hexane (0 °C). Optimum temperature of the collection solvent, ranging between 0 and −5 °C, was found to minimize loss of volatile hydrocarbons, while also preventing plugging of the restrictor line (which has been observed at very low temperatures of −40 °C).[15] Once extractions were terminated, bulk (unfractionated) extracts were subsequently concentrated to approximately 10 mL in a 125-ml pear flask using a vacuum rotary evaporator (Rotavap). Each extract was then transferred to a volumetric concentrator tube for evaporation to a final 5 mL volume using a nitrogen evaporator (N-EVAP). Each pear flask was rinsed three times with hexane, and all rinses added to the concentrator tube. Final 1:5 and 1:10 (extract:hexane) dilutions were necessary for the 3S sample extracts prior to analysis to prevent hydrocarbon peaks from saturating the GC-MS detector. Prior to analysis, 25 μL of a 1000 μg/mL perdeuterated internal standard solution was added to each 5 mL extract, containing *n*-dodecane-d_{26} (*n*-$C_{12}D_{26}$), *n*-hexadecane-d_{34} (*n*-$C_{16}D_{34}$), *n*-nonadecane-d_{40} (*n*-$C_{19}D_{40}$), and *n*-triacontane-d_{62} (*n*-$C_{30}D_{62}$) in equal amounts dissolved in hexane.

Triplicate extractions were performed on each sieve size for each sample as a measure of reproducibility. Quartz sand, previously baked in a muffle furnace at 450 °C for 6 h, was used as a method blank at the start of each batch of extractions (daily) to monitor for contamination. Each sample and method blank was spiked with a perdeuterated surrogate solution containing *n*-decane-d_{22} (*n*-$C_{10}D_{22}$) and *n*-tetracosane-d_{50} (*n*-$C_{24}D_{50}$) in hexane, just prior to the start of each extraction to estimate extraction efficiency. The *n*-$C_{10}D_{22}$ surrogate was chosen to monitor recovery of lower molecular weight, volatile hydrocarbons, while *n*-$C_{24}D_{50}$ was chosen to monitor recovery of higher molecular weight, low-volatility hydrocarbons.

Additional method validation extractions included a time study wherein the length of the dynamic step was evaluated over 0.5, 1, 2, and 3 h time segments.

This study used "Bone Dry" (99.9% minimum purity) CO_2 contained in a high-pressure cylinder equipped with a siphon (Airgas, Inc.). Nitrogen gas (HP grade) for the N-EVAP was also purchased from Airgas, Inc. All perdeuterated hydrocarbon surrogate and internal standards were purchased from Sigma-Aldrich, Inc., with stock solutions prepared in *n*-hexane (TraceSELECT, Sigma-Aldrich, Inc.). Quartz sand used for all method blanks was also purchased from Sigma-Aldrich, Inc.

Gas Chromatography−Mass Spectrometry Analysis. Quantitative analysis of total resolvable *n*-aliphatic hydrocarbons from all extracts was performed on an Agilent 6890 series gas chromatograph (GC) interfaced with an Agilent 5973 mass-selective detector (MSD). Automatic sample injection was performed with an Agilent 7683 Series Automatic Injector, operating in splitless mode to maximize resolution of trace compounds. The instrument was equipped with an HP-5MS capillary column (30 m × 0.25 mm × 0.25 μm). Operating conditions included (1) a 1 μL injection volume; (2) 0.9 mL/min carrier gas (He) flow rate; and (3) 50 °C initial oven temperature (holding for 1.5 min), followed by an oven temperature ramp to 315 °C at 10 °C/min, followed by a 15 min hold time at 315 °C.[56] The MSD operated in full-scan mode (35−500 amu). Target hydrocarbon peaks were identified by their GC retention times and mass spectral fragmentation patterns in comparison to standard compounds. Quantitative measurements were made from the signal intensity (total ion counts/second) for the area under the peak of the user-defined target ion (base peak, m/z = 57). An external seven-point calibration curve (0.25−10.0 μg/mL) was generated for an *n*-aliphatic hydrocarbon standard solution (*n*-C_9 through *n*-C_{40} in hexane), and a six-point calibration curve was generated for the surrogate standard solution (*n*-$C_{10}D_{22}$ and *n*-$C_{24}D_{50}$ in hexane). A quadratic regression model was used to establish the best fit relationship between concentration and response, with coefficient of determination (r^2) values ≥0.999 for *n*-C_9 through *n*-C_{30}. Calibration was checked with each batch of sample extracts. Helium (BIP grade) was purchased from Airgas, Inc. The *n*-C_7 through *n*-C_{40} saturated alkane mixture used for calibration was purchased from Sigma-Aldrich, Inc., with stock solutions prepared in *n*-hexane (TraceSELECT, Sigma-Aldrich, Inc.).

Brunauer−Emmett−Teller Surface Area Analysis. Specific surface area was measured on a subset of ground samples to evaluate differences in surface area among the sieve size fractions. One sample

DOI: 10.1021/acs.energyfuels.5b02059
Energy Fuels 2015, 29, 7897−7909

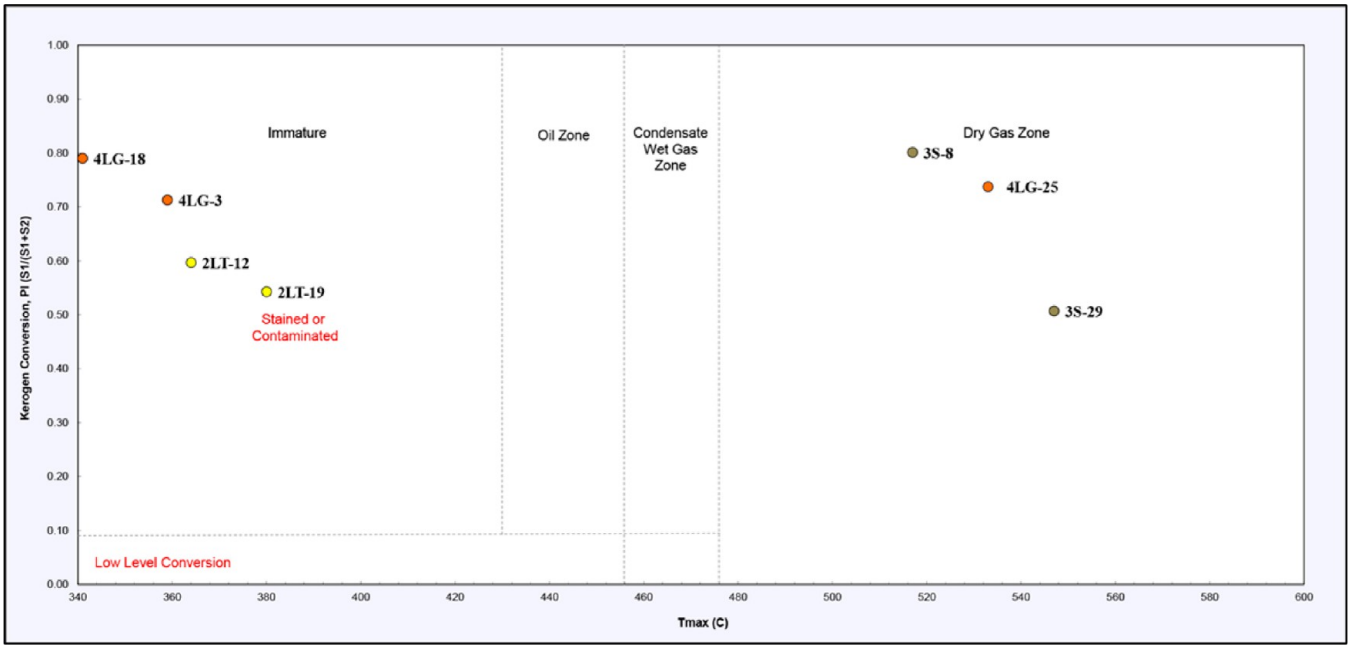

Figure 3. Kerogen conversion and maturity plot derived from Rock-Eval II pyrolysis data, relating production index (PI) to T_{max} values. Analyses performed by GeoMark Research, Ltd.

from each core (3S-8, 2LT-12, and 4LG-3) was analyzed (all sieve size fractions). Surface area analyses were performed by Particle Technology Labs on a Micromeritics TriStar II 3020 static pressure (volumetric) analyzer, with N_2 as the adsorbate gas. Accuracy for the BET surface area results is within ±0.24 m^2/g (±1%), which is within the range of accepted instrumental accuracy of ±3.45% (at the 99.7% confidence level). Uncertainties, determined from triplicate analyses, have been reported to within ±0.3 m^2/g (±1%, ±1 standard error of the mean, σ_m).

Scanning Electron Microscopy. SEM imaging was performed on a JEOL 8900 Electron Probe Microanalyzer at the University of Maryland to visualize and characterize the surface of sample particles within each sieve size fraction. Prior to analysis, samples were mounted on carbon tape and then coated with a thin layer of carbon fibers to minimize charging at the surface. Both secondary electron (SE) and back-scatter electron (BSE) images were taken of the 1000−500 μm and 250−125 μm sieve size fractions of sample 4LG-3.

Additional high-resolution SE images of shale pore structure were taken with a JEOL 5800-LV field emission scanning electron microscope (FESEM) at the USGS Denver Microbeam Laboratory. Prior to analysis, sample chips (one from each core) were polished, ion-milled, and carbon-coated using a carbon evaporator.

RESULTS

Rock-Eval II Pyrolysis and TOC Analysis. Rock-Eval II pyrolysis was used as an initial screening technique to evaluate the quantity, quality, and thermal maturity of organic matter in 31 shale samples. Quantity of organic matter, or organic richness, was evaluated based upon TOC content, which is composed of the pyrolyzable carbon fraction (S1 and S2) and the residual carbon fraction.[45] The S1 and S1/TOC parameters were the key criteria used to screen samples for subsequent solvent extractions. Although S1 does not correspond directly to solvent-extracted organic matter,[31,45] this parameter is a crude approximation of potentially extractable hydrocarbon content. The seven samples selected for the supercritical CO_2 extractions had the highest S1 and S1/TOC values of the initial sample set (Table 1).

Very low hydrogen index (HI ≡ S2/TOC) values (<50 mg HC/g TOC) and oxygen index (OI ≡ S3/TOC) values (<39 mg CO_2/g TOC) were found for all samples. A modified Van Krevelen diagram suggests that the type of kerogen present could be oxidized, highly mature, or Type IV kerogen.[45,57] However, low HI (0−100) and OI (5−30) values of other Devonian shales in the Appalachian Basin are suggested to represent original Type II organic matter converted to Type IV (inert solid bitumen) by a high degree of thermal maturation.[58]

Thermal maturity, which can be roughly estimated from T_{max} and production index (PI ≡ S1/(S1+S2)) measurements, indicates the degree to which kerogen is transformed into free hydrocarbons.[45,46] Sample PI values range from 0.5 to 0.8, which suggests they are in a late-mature/post-mature stage of hydrocarbon generation, the dry gas window, occurring at subsurface paleotemperatures of approximately 150−200 °C.[45] Yet, T_{max} values for the 2LT core samples (2LT-12 and 2LT-19) and two out of three of the 4LG core samples (4LG-3 and 4LG-18) are suggestive of immature sediments, which is not in agreement with associated PI values for those samples. A kerogen conversion and maturity plot (Figure 3) suggests that those samples are potentially "stained or contaminated", whereas the three other samples plot within the dry gas zone (3S-8, 3S-29, and 4LG-25). Sample pyrograms, however, are not characteristic of contaminated reservoir rocks, either by oil-based or water-based additives, lubricants, or natural, migrated oil.[45] There is also no distinctive feature of the pyrograms distinguishing two groups of samples (dry gas zone versus stained/contaminated). Thus, although possible contamination cannot be ruled out for the samples in this study, the low S1 and S2 peak values, and low derived HI, suggest that the likelihood of contamination is low. Furthermore, given the low S2 peaks, S2 and T_{max} values are often inaccurate, as are derived Rock-Eval parameters (i.e., PI and HI), and should be supported by additional geochemical analyses.[45]

Organic Petrography. Reflectance measurements of the observable organic matter, ranging from 2.2 to 2.6 (±0.5) $\%R_o$

DOI: 10.1021/acs.energyfuels.5b02059
Energy Fuels 2015, 29, 7897−7909

Table 2. Reflectance Analysis Measurements of Solid Bitumen (Pyrobitumen)

sample ID	no. of measurements	mean (%R_o)	uncertainty[a] (±%R_o)	relative uncertainty (%)
3S-8	24	2.3	0.3	15
2LT-12	21	2.6	0.5	18
4LG-3	23	2.2	0.4	17

[a]Uncertainties are reported as ±1σ.

(Table 2), confirm a high degree of thermal maturity for the shale samples (dry gas window). These reflectance values are slightly higher than those reported on regional thermal maturity maps (approximately 1.3−2 %R_o) for Appalachian Basin Devonian shales in the counties wherein these cores were drilled.[44,58,59] However, given the uncertainties for these measurements, there is no significant difference among thermal maturity values. Thermal maturity zones reported across the Appalachian Basin are also compiled from both reflectance (%R_o) and conodont color alteration index (CAI) measurements taken on different samples within the basin, and currently there is no conversion factor between the two indices.[44]

Reflectance measurements also reveal the predominant form of organic matter to be solid pyrobitumen, as evidenced by its pore-lining and pore-filling texture, and growth around mineral grains (Figure 4).[60,61] The principal type of original organic

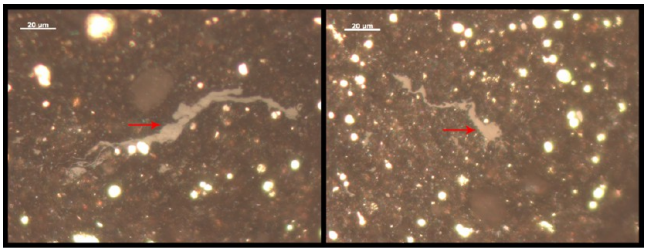

Figure 4. Reflectance images of pyrobitumen. Red arrows point to pyrobitumen within the shale matrix. Bright framboidal pyrite structures are dispersed throughout. Left: 3S-8, with a reflectance value of 2.6 %R_o. Right: 2LT-12, with a reflectance value of 3.0 %R_o.

matter, Type II kerogen (*Tasmanites* algae, a telalginite maceral, and bituminite macerals), was inferred from studies of other low-maturity Marcellus Shale and Devonian-age shales elsewhere in the Appalachian Basin.[58,62]

XRD. The XRD results show that all samples are composed of primarily quartz (24−40%) and clay (mainly illite) minerals (12−62%) (Figure 5, Tables 3 and 4). Carbonate minerals are only abundant in samples 3S-29 (46%) and 4LG-18 (36%). Minor mineral constituents (<10% and ≥5%) include pyrite and chlorite. Feldspars are present in trace quantities (<5%). The mineralogy is similar to that reported for other Marcellus Shale samples.[25,62−64]

Supercritical CO_2 Extractions: Distribution of Extracted Hydrocarbons. Supercritical CO_2 extracted *n*-aliphatic hydrocarbons in the range of predominantly *n*-C_{11} through *n*-C_{21}, with highest recovery between *n*-C_{12} and *n*-C_{15}. No significant difference is observed in the distribution of extracted *n*-aliphatic hydrocarbons between sieve size fractions for a given sample, or between samples within a given core. However, a few distinctions are noticeable among cores (Figure 6). Only hydrocarbons *n*-C_{11} through *n*-C_{14} are present in the 3S sample extracts. The 2LT and 4LG sample extract chromatograms reveal additional compounds, including branched aliphatic hydrocarbons. All 4LG sample extracts

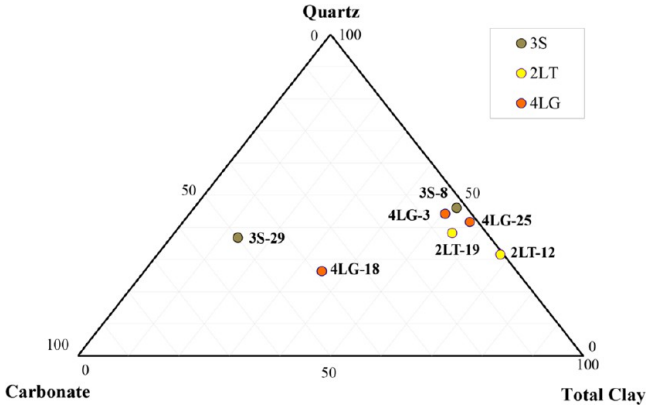

Figure 5. Ternary diagram showing the relative proportions of total clay, carbonate and quartz in each sample.

contain *n*-aliphatic hydrocarbons ranging from approximately *n*-C_{11} through *n*-C_{21}. The 2LT sample extracts have a tighter distribution range of resolvable *n*-aliphatic hydrocarbons (*n*-C_{11} through *n*-C_{14}), yet a broad unresolved complex mixture (UCM) is also evident with qualitatively identifiable *n*-aliphatic peaks ranging from approximately *n*-C_{18} through *n*-C_{23}. The source and chemical composition of the UCM is unknown, but previous work suggests the UCM may result from petroleum compounds resistant to chemical and biological degradation, or from different sources of petroleum contamination.[65] However, the Rock-Eval II data (Table 1) and pyrograms discussed above provide supporting evidence that the likelihood of contamination (by drilling additives or natural, non-indigenous hydrocarbons) is low.

Supercritical CO_2 Extractions: Quantity of Extracted Hydrocarbons. The quantity of extracted total resolvable, *n*-aliphatic hydrocarbons ranges from approximately 0.01 to 0.6 parts per thousand by weight (mg HC/g rock), or 0.3−12 (mg HC/g TOC). Results indicate an order of magnitude increase in yield from the 3S extracts (all sieve size fractions), in comparison to that recovered from the 2LT and 4LG extracts (Figure 7). Extraction results also reveal a trend among all samples with regard to sieve size, showing a slight increase in hydrocarbon yield from the intermediate (250−125 μm) sieve size fraction, followed by a drop in yield from the 63−25 μm sieve size fraction.

Relative uncertainty, i.e., the ratio of the standard error of the mean (σ_m) to the average, expressed as a percent, was used to evaluate precision. Measurement uncertainties range between ±2 and 11% for each set of triplicate extractions performed on each sieve size fraction for a given sample. For most of the extractions, *n*-C_{11} through *n*-C_{13} have the highest deviation and contribute the largest source of error to the overall results. Slight fluctuations in the volume of CO_2 dispensed in each extraction (70−90 mL) among replicate extractions may have also contributed a source of variability. Surrogate standard recovery totals, averaged across all extractions (samples and method blanks), are 47 ± 3% for *n*-$C_{10}D_{22}$ and 97 ± 2% for *n*-

DOI: 10.1021/acs.energyfuels.5b02059
Energy Fuels 2015, 29, 7897−7909

Table 3. Nomenclature for XRD Results

label	mineral name(s)	mineral formula(s)
QTZ	quartz	SiO_2
FLD	K-feldspar and Plagioclase (albite to anorthite)	$KAlSi_3O_8$ and $NaAlSi_3O_8$ (albite) to $CaAl_2Si_2O_8$ (anorthite)
CARB	calcite, ankerite, dolomite, and siderite	$CaCO_3$, $Ca(Fe^{2+},Mg)(CO_3)_2$, $CaMg(CO_3)_2$, and $FeCO_3$
I/S	illite/smectite	$K_yAl_4(Si_{8-y}, Al_y)O_{20}(OH)_4$ $(1 < y < 1.5)/(1/2Ca,Na)(Al,Mg,Fe)_4(Si,Al_8O_{20}(OH)_4{\cdot}nH_2O)$
KAOL	kaolinite	$Al_2Si_2O_5(OH)_4$
CHLR	chlorite	$Mg_2Al_2SiO_5(OH)_4$
PY	pyrite, marcasite, and sphalerite	FeS_2, FeS_2, and (Zn,Fe)S
other	trace (low-level qualitative ID)	N/A

Table 4. Major (≥50%), Minor (<10% and ≥5%), and Trace (<5%) Phase Mineralogy

sample ID	QTZ	FLD	CARB	I/S	I	KAOL	CHLR	PY	other	total clay
3S-8	40.4	1.8	1.8	0.0	37.0	0.0	8.5	9.6	0.8	45.5
3S-29	34.1	1.5	46.3	0.0	12.3	0.0	0.0	4.3	0.0	12.3
2LT-12	28.9	1.9	0.6	0.0	51.3	0.0	10.8	6.0	0.0	62.1
2LT-19	33.0	2.2	5.9	0.0	45.4	0.0	2.0	9.7	0.3	47.4
4LG-3	39.7	2.7	4.7	0.0	36.0	0.0	9.4	7.1	0.0	45.4
4LG-18	24.4	0.7	35.7	0.0	27.7	0.0	4.8	5.8	0.0	32.5
4LG-25	36.1	2.4	1.4	0.0	43.1	0.0	6.0	9.8	0.6	49.1
uncertainty[a] (±%)	0.7	0.5	0.2	0.0	0.4	0.0	0.5	0.8	0.1	0.7

[a]Uncertainties are reported within $\pm 1\sigma$.

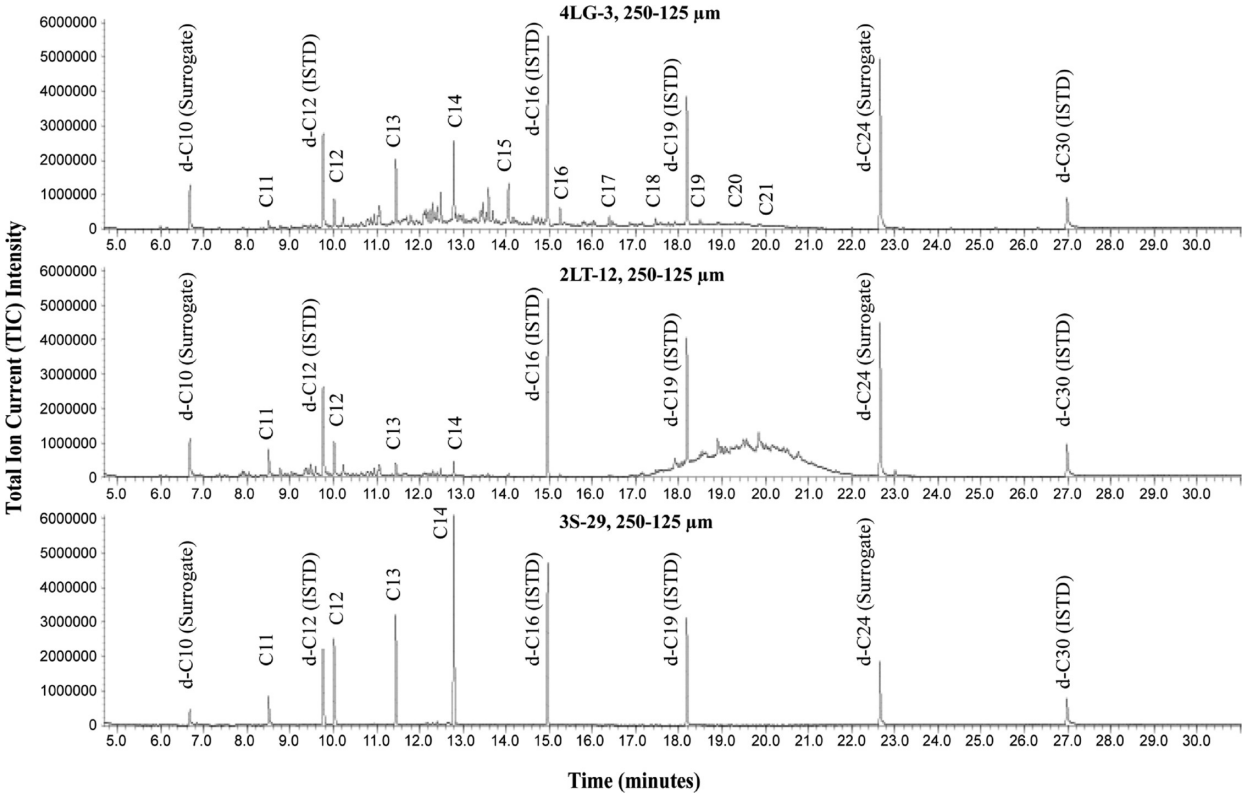

Figure 6. Total ion current chromatograms of representative samples from each core. Chromatograms highlight the difference in distribution of extracted *n*-aliphatic hydrocarbons between cores.

$C_{24}D_{50}$. Uncertainties for surrogate standards are reported as $\pm 1\sigma_m$. Higher volatility of the lower molecular weight surrogate (n-$C_{10}D_{22}$), and of target hydrocarbons of similar molecular weight, may make them more sensitive to loss in postextraction (solvent evaporation) steps in this extraction method, accounting for lower-than-expected yields.[21,66]

To examine whether extraction time had an effect on the quantity or distribution of extracted hydrocarbons, a series of extractions were performed wherein the time of the dynamic step was changed from 1 h to 30 min, 2 h, and 3 h increments. Sample splits from the 4LG-25, 250−125 μm fraction were used in each extraction. Results (Figure 8, Table 5) identify highest recovery from the 1 h dynamic step, wherein the average volume of CO_2 dispensed in the triplicate extractions is approximately 86 mL. The 30 min dynamic step yielded the lowest recovery. Results suggest that extraction yield is

DOI: 10.1021/acs.energyfuels.5b02059
Energy Fuels 2015, 29, 7897−7909

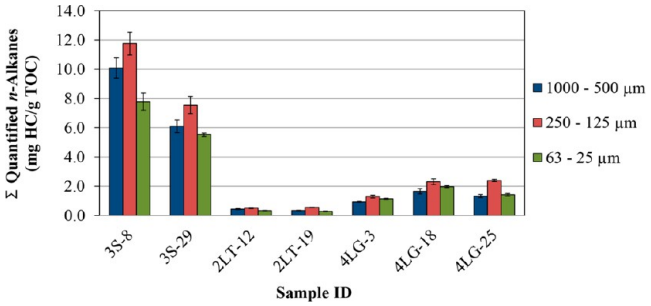

Figure 7. Supercritical CO_2 extractions: Total quantity of resolvable *n*-aliphatic hydrocarbons extracted from each sample as a function of sieve size. Error bars are $\pm 1\sigma_m$.

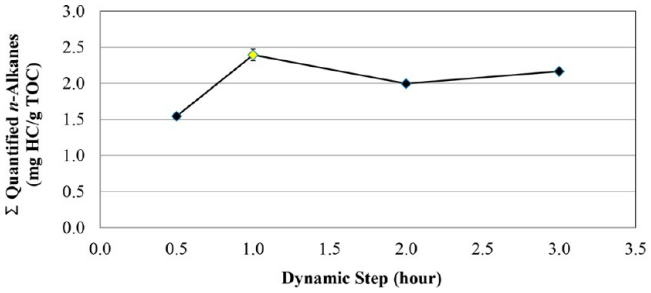

Figure 8. Relationship between extraction time and hydrocarbon yield for the supercritical CO_2 extractions. The length of the dynamic (flow through) step was varied for sample 4LG-25, 250−125 μm sieve size. The reported value for the 1 h extraction is an average value from triplicate extractions with an uncertainty of ±0.1 mg HC/g TOC ($\pm 1\sigma_m$). Only one extraction was performed for the 30 min, 2 h, and 3 h extractions. Results show a 43% increase in hydrocarbon yield by increasing the length of time for the dynamic step from 30 min to 1 h. A decrease in yield was then observed as the dynamic step was extended to 2 h and 3 h intervals (18% and 10% decline in yield, relative to the 1 h interval, respectively).

Table 5. Percent Difference in Extraction Yield as a Function of Time

dynamic step duration (h)	total quantified *n*-alkanes (mg HC/g TOC)
0.5	1.5
1	2.4
2	2.0
3	2.2

optimized with the 1 h dynamic step used in our supercritical CO_2 extractions.

Surface Area Analysis and SEM Imaging. Surface area results do not reveal any significant variation nor consistent trend among sieve sizes (Figure 9, Table 6). However, subsequent SEM images reveal that individual crushed shale particles within each sieve size fraction are coated in a layer of smaller adhered fine particles (Figures 10 and 11). Thus, the sieve size fractions used in this study are merely sieve size ranges and not a true indication of rock matrix grain size distribution.

Additional FESEM images (Figure 12) reveal a mixed-pore network for each sample (3S-8, 2LT-12, and 4LG-3), including nanometer-size pores associated with both the organic matter and the mineral matrix (interparticle and intraparticle) using Loucks et al.'s[26] pore type classification for mudrocks. Pores present within the organic matter are heterogeneous in distribution and shape, ranging from simple spheroid and

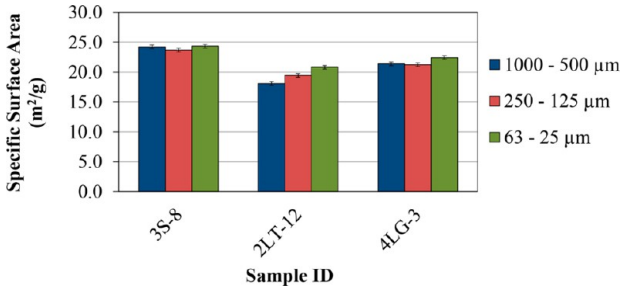

Figure 9. Specific surface area results. Results from each sample are reported as a function of sieve size. Error bars are $\pm 1\sigma_m$.

Table 6. BET Specific Surface Area Results

sample ID	sieve size (μm)	specific surface area (m^2/g)	uncertainty[a] (±m^2/g)	relative uncertainty (%)
3S-8	1000−500	24.2	0.3	1
	250−125	23.7	0.3	1
	63−25	24.3	0.3	1
2LT-12	1000−500	18.1	0.3	2
	250−125	19.5	0.3	2
	63−25	20.8	0.3	1
4LG-3	1000−500	21.4	0.3	1
	250−125	21.2	0.3	1
	63−25	22.4	0.3	1

[a]Reported uncertainties are $\pm 1\sigma_m$.

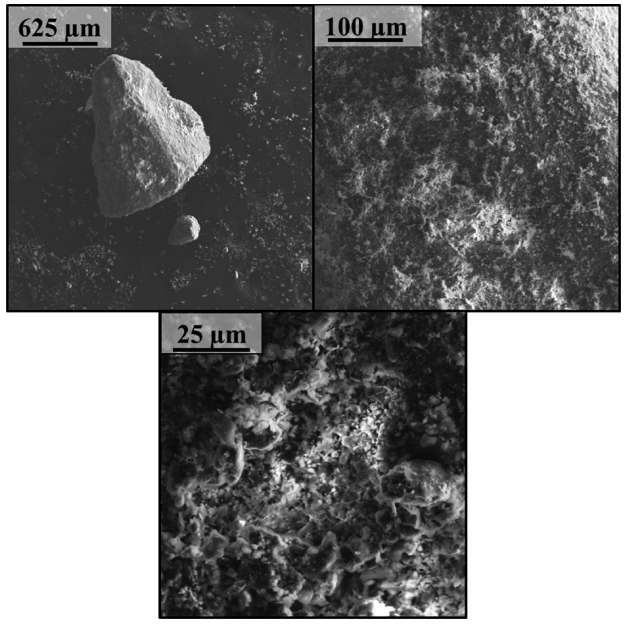

Figure 10. SEM images of 4LG-3, 1000−500 μm sieve size fraction. Magnification: top left, 40×; top right, 250×; and bottom, 1000×.

elliptical structures to more complex, irregular shapes. The interparticle pores (intergranular and intercrystalline) have no visible preferred orientation, with a variety of shapes ranging from elongated, elliptical pores to triangular and more complex, irregular void spaces. Intraparticle pores are visible as intercrystalline pores within pyrite framboids (Figure 12,

DOI: 10.1021/acs.energyfuels.5b02059
Energy Fuels 2015, 29, 7897−7909

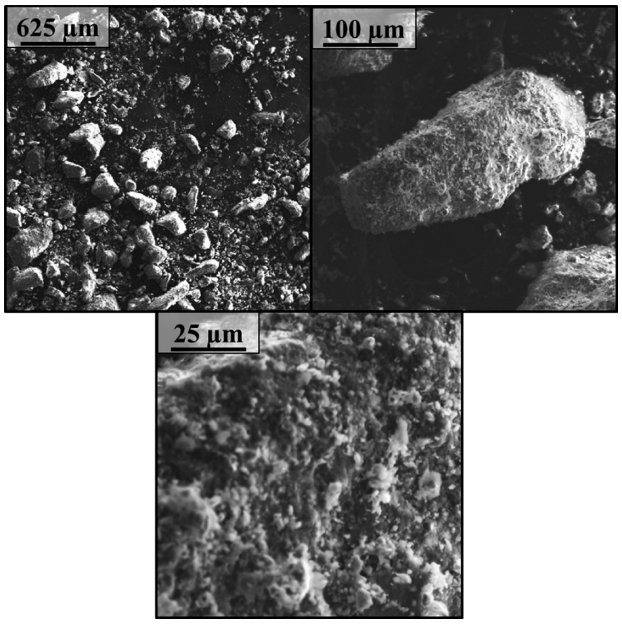

Figure 11. SEM images of 4LG-3, 250−125 μm sieve size fraction. Magnification: top left, 40×; top right, 250×; and bottom, 1000×.

bottom right), dissolution pores around the rim of an unidentified mineral (Figure 12, bottom right), and within aggregates of clay grains (Figure 12, bottom left).

DISCUSSION

Extracted Hydrocarbons. The total yield of extracted *n*-aliphatic hydrocarbons ranges from approximately 0.3 to 12 mg HC/g TOC, with lowest recovery from the 2LT samples and highest recovery from the 3S samples. The overall distribution of extracted *n*-aliphatic hydrocarbons ranges from predominantly *n*-C_{11} through *n*-C_{21}, with highest yields between *n*-C_{12} and *n*-C_{15}. A greater proportion of aliphatic hydrocarbons with carbon number < C_{19} are generated from high-maturity samples, relative to heavier C_{19+} hydrocarbons typically associated with thermally immature samples, likely due to an increase in the degree of thermal degradation of organic matter associated with advanced levels of maturity.[58] The distribution of hydrocarbons recovered in this study is also comparable to previous supercritical CO_2 extraction studies wherein organic matter was extracted from petroleum source rocks under similar extraction conditions.[14,15,18]

No apparent differences are observed among cores with regard to organic matter content, mineralogy, or surface area and pore imaging analyses that could account for the discrepancies in the quantity or distribution of extracted hydrocarbons. The Rock-Eval II data (Table 1) and pyrograms also support the interpretation that the likelihood of contamination in these samples is low. Thus, the extracted hydrocarbons most likely reflect naturally occurring, residual organic matter present within the shale matrix.

Lower yields observed in the supercritical CO_2 extractions compared to S1 (and S1/TOC) values measured via Rock-Eval II pyrolysis (Table 1) are expected given sample preparation and procedural differences between the two extraction techniques. Solvent extractions typically cause greater loss of lower molecular weight, more volatile hydrocarbons, relative to pyrolysis, largely due to solvent evaporation prior to analysis. Solvent-extracted organic matter is also dependent upon solvent polarity and extraction parameters.[45,67] Additionally, only the resolvable *n*-aliphatic hydrocarbons, a fraction of the bulk extract, were quantified in our supercritical CO_2 extractions.

No strong correlation was established between hydrocarbon yield and sieve size. However, a trend is observed in all sample extracts, with highest recovery from the 250−125 μm sieve size fraction. The effect of sieve sieve size on extraction yield may not be as significant as was initially expected. Lack of a significant relationship could have been obscured by the coating of adhered fine particles discovered on all individual crushed shale particles (Figures 10 and 11), suggesting an overlap of rock matrix grain sizes across the sieve size fractions. Further considerations include loss of volatile compounds upon crushing the shale, and potential channeling and particle aggregation effects, especially within the 63−25 μm fraction, all of which could have reduced extraction rates and overall recovery.[20,35,36,38]

Additional steric limitations may also have a substantial effect on hydrocarbon yield among particle sizes. The Marcellus and other Devonian shales have pore and pore throat sizes on the order of 10^{-1}−10^{-3} μm in diameter.[24,25] Thus, with an effective molecular diameter of 3.3 Å (3.3 × 10^{-4} μm),[22] CO_2 can access nanometer-size pores of shale matrices. However, some petroleum hydrocarbon constituents can have molecular diameters (roughly 5−50 Å for asphaltene molecules/aggregates down to 3.8 Å for methane)[22,24,68] of approximately the same order of magnitude as characteristic shale pore and pore throat sizes, 10^{-2}−10^{-4} μm.[22,24−26] Thus, although CO_2 can access particle surface porosity and solvate potentially extractable hydrocarbons, the resultant supercritical fluid mixture may not be able to effectively navigate through/out of the shale porosity network. If this is the case, a threshold of hydrocarbon extraction may have been reached, contributing to a lack of trend among sieve size fractions.

Effect of Surface Area and Porosity. No clear inverse relationship was observed between surface area and particle size for this sample set. One potential factor contributing to the lack of significant variation of surface area among the designated sieve size ranges is the coating of adhered fine particles found on all individual crushed shale particles, as discussed above (Figures 10 and 11).

Another potential explanation is that different techniques for characterizing surface area and porosity (i.e., low-pressure N_2 and CO_2 gas adsorption, mercury intrusion, helium porosimetry, and small-angle neutron scattering/ultra-small-angle neutron scattering (SANS/USANS) techniques can yield different results. Varying results of gas adsorption techniques in particular may reflect the size and shape of both the adsorbate gas molecules and pores of the adsorbent surface, accessibility of the adsorbing gas to the pores, and molecular interactions between the gas and sample surface.[27,28,69,70]

Nitrogen, with a molecular cross-sectional area of 0.162 nm^2 (at 77 K) is considered a widely suitable adsorptive gas for measuring surface area, resulting in BET surface areas within 20% of true surface areas.[69] However, at 77 K (−196 °C), N_2 has insufficient thermal energy to diffuse through narrow pore networks. Alternatively, CO_2 (0.251 nm^2 molecular cross-sectional area), used in adsorption analyses at a higher temperature (273 K, 0 °C), has the necessary thermal energy to access a microporous adsorbent.[71] Whereas both N_2 and CO_2 can access mesopores (2−50 nm) of shale and coal matrices, micropores (<2 nm) are more accessible to CO_2.[28]

DOI: 10.1021/acs.energyfuels.5b02059
Energy Fuels 2015, 29, 7897−7909

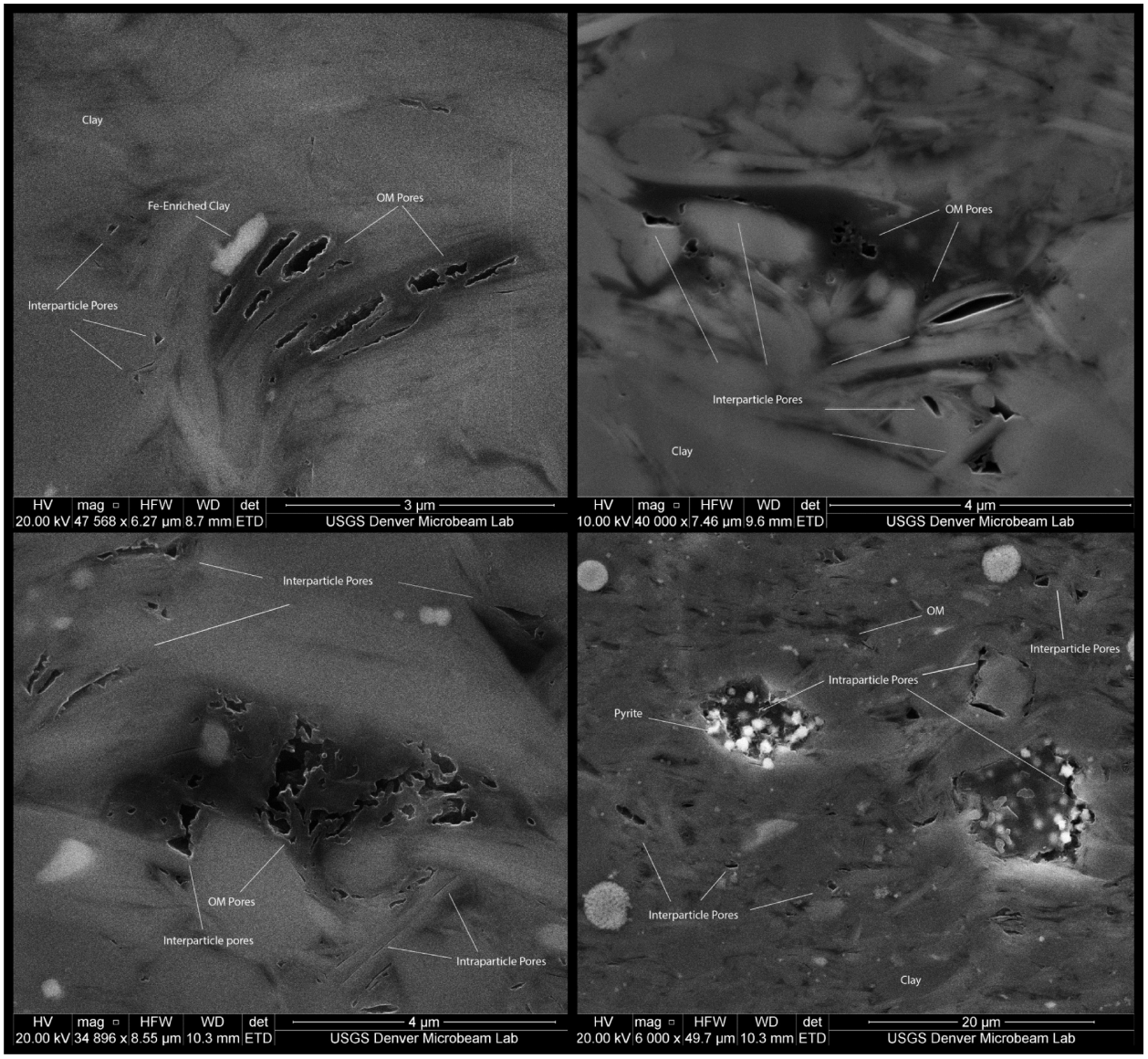

Figure 12. SEM images taken from the FESEM analysis of pore structure: top left, 3S-8; top right, 4LG-3; bottom left, 2LT-12; and bottom right, 2LT-12.

Consequently, surface areas measured with CO_2 are often 1−2 orders of magnitude larger than those measured with N_2.[71] A comparison of these adsorption methods on mature shale and other source rocks likewise show an increase in specific surface area when measured with CO_2, depending upon the abundance of micropores associated with organic matter.[27−29] Thus, the use of N_2 to measure surface area in this study may be obscuring a potential trend of exposed surface area with particle size. Accordingly, supercritical CO_2 may be accessing and extracting hydrocarbons from pores not detected by N_2-derived surface area measurements or SEM imaging, subsequently obscuring a more accurate relationship of extraction yield as a function of surface area, regardless of sieve size range (Figure 13).

Nevertheless, a plot of surface area as a function of TOC content (Figure 14) shows a positive correlation between the two variables. Previous studies have also found positive correlations between both mesoporosity and microporosity (surface areas and volumes) and TOC content in shales, suggesting that porosity within organic matter is significant.[27−29,72−74] Given that extraction yield also increases with increasing TOC content (Figure 15), the exposed internal surface area of pores associated with organic matter may be an important controlling factor on extraction yield.

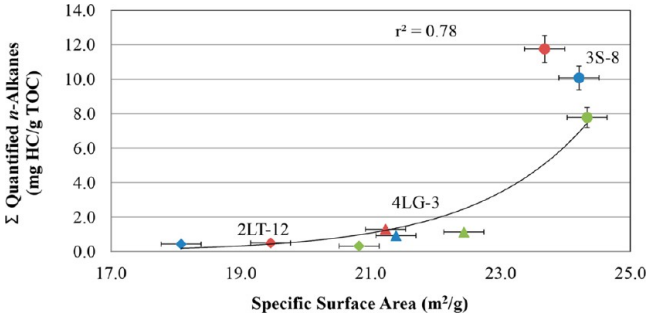

Figure 13. Extraction yield as a function of specific surface area. Vertical and horizontal error bars are $\pm 1\sigma_m$. Samples: 3S-8 (circles), 4LG-3 (triangles), 2LT-12 (diamonds). Sieve ranges: 1000−500 μm (blue), 250−125 μm (red), and 63−25 μm (green).

DOI: 10.1021/acs.energyfuels.5b02059
Energy Fuels 2015, 29, 7897−7909

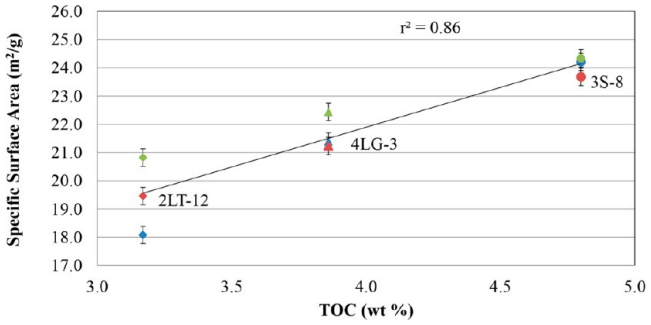

Figure 14. Specific surface area as a function of TOC. Vertical error bars are $\pm 1\sigma_m$. Samples: 3S-8 (circles), 4LG-3 (triangles), 2LT-12 (diamonds). Sieve ranges: 1000−500 μm (blue), 250−125 μm (red), and 63−25 μm (green).

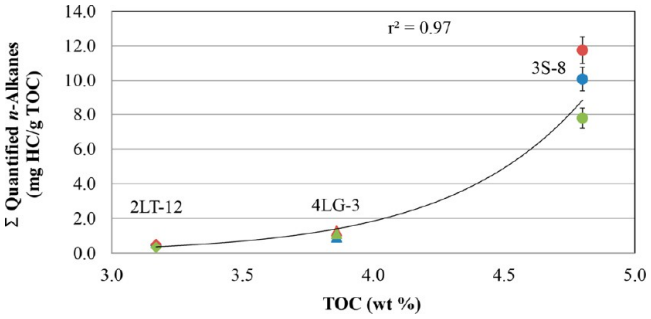

Figure 15. Extraction yield as a function of TOC. Vertical error bars are $\pm 1\sigma_m$. Samples: 3S-8 (circles), 4LG-3 (triangles), 2LT-12 (diamonds). Sieve ranges: 1000−500 μm (blue), 250−125 μm (red), and 63−25 μm (green).

CONCLUSIONS

(1) Supercritical CO_2 can liberate diesel-range *n*-aliphatic hydrocarbons from high-maturity shale at estimated *in situ* reservoir pressure and temperature conditions. Extraction yields range between 0.3 and 12 mg HC/g TOC.

(2) No strong correlation is found between sieve size and extracted hydrocarbon yield. However, hydrocarbon yield is highest from the 250−125 μm sieve size fraction in all sample extracts. The significance of the effect of sieve size on yield may have been limited given the low sieve size ranges of the extracted shale particles.

(3) Mineralogy appears to have no effect on the observed differences in extraction yield (abundance or distribution of hydrocarbons) among cores.

(4) Extraction yield increases with increasing surface area, regardless of sieve size range. However, given N_2's inability to access micropores (<2 nm) within shale matrices, use of N_2 as opposed to CO_2 to measure surface area may be obscuring a stronger correlation between extraction yield and exposed surface area.

(5) Surface area and extraction yield both increase with an increase in TOC content, reflecting the contribution of organic matter to pores and exposed internal surface areas within the shale matrix that are accessible to the extraction solvent, supercritical CO_2.

AUTHOR INFORMATION

Corresponding Author

*E-mail: pjarboe@usgs.gov.

Present Address

⊥For P.J.J.: U.S. Geological Survey, 12201 Sunrise Valley Dr., MS 956, Reston, VA 20192

Notes

Disclosure. Any use of trade, product, or firm names is for descriptive purposes only and does not imply endorsement by the U.S. Government or the University of Maryland.

The authors declare no competing financial interest.

ACKNOWLEDGMENTS

This project was funded by the ACS-PRF's New Directions Grant 52387-ND8, the 2013 PAPG Named Grant, sponsored by the AAPG Foundation's Grants-in-Aid program, the UMD Green Fellowship in Global Climate Change, and the USGS's Energy Resources Program. Samples were provided courtesy of EXCO Resources, Inc., and the Pennsylvania Geological Survey, Department of Conservation and Natural Resources. The authors thank UMD faculty and staff, Drs. Phil Piccoli and Michael Evans, and Rebecca Plummer. Considerable gratitude also goes to USGS scientists and colleagues Jon Kolak, Leslie Ruppert, Dave Houseknecht, Robert Burruss, Peter Warwick, Paul Hackley, Frank Dulong, Heather Lowers, Terry Lerch, William Orem, Margo Corum, Matthew Varonka, Joseph East, Eric Morrissey, Nicholas Geboy, and John Jackson, for all of their support, collaboration, and laboratory resources. The authors also thank the anonymous reviewers for their insightful comments on the manuscript. Additional acknowledgements go to UMD students Brittney Gaeta and Harrison Lisabeth for laboratory assistance throughout the project.

REFERENCES

(1) Lee, D. S.; Herman, J. D.; Elsworth, D.; Kim, H. T.; Lee, H. S. *KSCE J. Civ. Eng.* **2011**, *15* (4), 679−687.

(2) Middleton, R. S.; Carey, J. W.; Currier, R. P.; Hyman, J. D.; Kang, Q.; Karra, S.; Jiménez-Martínez, J.; Porter, M. L.; Viswanathan, H. S. *Appl. Energy* **2015**, *147*, 500−509.

(3) Abdallah, W.; Buckley, J.; Carnegie, A.; Edwards, J.; Herold, B.; Fordham, E.; Graue, A.; Habashy, T.; Seleznev, N.; Signer, C.; Hussain, H.; Montaron, B.; Ziauddin, M. *Schlumberger Oilfield Rev.* **2007**, *19* (2), 44−61.

(4) Wang, H.; Li, G.; Shen, Z. *Energy Sources, Part A* **2012**, *34* (15), 1426−1435.

(5) Oldenburg, C. M.; Pruess, K.; Benson, S. M. *Energy Fuels* **2001**, *15* (2), 293−298.

(6) Nuttall, B. C.; Eble, C. F.; Drahovzal, J. A.; Bustin, R. M. *Analysis of Devonian black shales in Kentucky for potential carbon dioxide sequestration and enhanced natural gas production*; Final Report, DOE Cooperative Agreement No. DE-FC26-02NT41442; Kentucky Geological Survey: Lexington, KY, 2005.

(7) Nuttall, B. C. *Reassessment of CO_2 sequestration capacity and enhanced gas recovery potential of Middle and Upper Devonian Black Shales in the Appalachian Basin*; MRCSP Phase II Topical Report, DOE Cooperative Agreement No. DE-FC26-05NT42589; OCDO Grant Agreement No. DC-05-13; Kentucky Geological Survey: Lexington, KY, 2010.

(8) Parris, T. M.; Greb, S. F.; Nuttall, B. C. *Evaluation of geologic CO_2 sequestration potential and CO_2 enhanced oil recovery in Kentucky*; Report of Investigations 21, Series XII; Kentucky Geological Survey: Lexington, KY, 2010.

(9) Sorensen, J.; Harju, J.; Hawthorne, S.; Braunberger, J.; Liu, G.; Smith, S.; Steadman, E. Concepts for CO_2 EOR in the Bakken Formation. Presented at the 19th Annual CO_2 Flooding Conference, Midland, Texas, December 9−13, 2013.

(10) Godec, M.; Koperna, G.; Petrusak, R.; Oudinot, A. *Int. J. Coal Geol.* **2013**, *118*, 95−104.

(11) Fathi, E.; Akkutlu, I. Y. *Int. J. Coal Geol.* **2014**, *123*, 52−61.

DOI: 10.1021/acs.energyfuels.5b02059
Energy Fuels 2015, 29, 7897−7909

(12) Maddocks, R. R.; Gibson, J.; Williams, D. F. *Chem. Eng. Prog.* **1979**, *75* (6), 49−55.
(13) Williams, D. F. *Chem. Eng. Sci.* **1981**, *36* (11), 1769−1788.
(14) Monin, J. C.; Barth, D.; Perrut, M.; Espitalié, M.; Durand, B. *Org. Geochem.* **1988**, *13* (4−6), 1079−1086.
(15) Li, W.; Lazar, I. M.; Wan, Y. J.; Butala, S. J.; Shen, Y.; Malik, A.; Lee, M. L. *Energy Fuels* **1997**, *11* (5), 945−950.
(16) Rudzinski, W. E.; Aminabhavi, T. M. *Energy Fuels* **2000**, *14* (2), 464−475.
(17) Span, R.; Wagner, W. *J. Phys. Chem. Ref. Data* **1996**, *25* (6), 1509−1596.
(18) Greibrokk, T.; Radke, M.; Skurdal, M.; Willsch, H. *Org. Geochem.* **1992**, *18* (4), 447−455.
(19) Jaffréa, R.; Gong, Y.; Furton, K. *J. High Resolut. Chromatogr.* **1997**, *20*, 586−590.
(20) Kolak, J. J.; Burruss, R. C. *An organic geochemical assessment of CO_2-coal interactions during sequestration*; Open-File Report 03-453; U.S. Geological Survey: 2003.
(21) Kolak, J. J.; Burruss, R. C. *Org. Geochem.* **2014**, *73*, 56−69.
(22) Tissot, B. P.; Welte, D. H. Physicochemical Aspects of Primary Migration. *Petroleum Formation and Occurrence: A New Approach to Oil and Gas Exploration*; Springer-Verlag: Berlin/Heidelberg, Germany, 1978; pp 260−284.
(23) Walker, P. L., Jr.; Verma, S. K.; Rivera-Utrilla, J.; Davis, A. *Fuel* **1988**, *67* (12), 1615−1623.
(24) Nelson, P. H. *AAPG Bull.* **2009**, *93* (3), 329−340.
(25) Chalmers, G. R.; Bustin, R. M.; Power, I. M. *AAPG Bull.* **2012**, *96* (6), 1099−1119.
(26) Loucks, R. G.; Reed, R. M.; Ruppel, S. C.; Hammes, U. *AAPG Bull.* **2012**, *96* (6), 1071−1098.
(27) Ross, D. J. K.; Bustin, R. M. *Mar. Pet. Geol.* **2009**, *26*, 916−927.
(28) Mastalerz, M.; He, L.; Melnichenko, Y. B.; Rupp, J. A. *Energy Fuels* **2012**, *26*, 5109−5120.
(29) Kuila, U.; McCarty, D. K.; Derkowski, A.; Fischer, T. B.; Topór, T.; Prasad, M. *Fuel* **2014**, *135*, 359−373.
(30) Etminan, S. R.; Javadpour, F.; Maini, B. B.; Chen, Z. *Int. J. Coal Geol.* **2014**, *123*, 10−19.
(31) Jarvie, D. Shale resource systems for oil and gas: Part 2—Shale-oil resource systems. In *Shale reservoirs: Giant resources for the 21st century*; Breyer, J. A., Ed.; AAPG Memoir 97; American Association of Petroleum Geologists: Tulsa, OK, 2012; pp 89−119, DOI: 10.1306/13321447M973489.
(32) Asep, E. K.; Jinap, S.; Tan, T. J.; Russly, A. R.; Harcharan, S.; Nazimah, S. A. H. *J. Food Eng.* **2008**, *85*, 450−458.
(33) Nagy, B.; Simándi, B. *J. Supercrit. Fluids* **2008**, *46*, 293−298.
(34) Allawzi, M.; Al-Otoom, A.; Allaboun, H.; Ajlouni, A.; Al Nseirat, F. *Fuel Process. Technol.* **2011**, *92*, 2016−2023.
(35) Reverchon, E.; De Marco, I. *J. Supercrit. Fluids* **2006**, *38*, 146−166.
(36) Martínez, J. L.; Vance, S. W. Supercritical Extraction Plants. In *Supercritical Fluid Extraction of Nutraceuticals and Bioactive Compounds*; Martínez, J. L., Ed.; CRC Press, Taylor & Francis Group: Boca Raton, FL, 2008; pp 28−31.
(37) Azzam, F. O.; Fullerton, K. L.; Kesavan, S.; Lee, S. *Fuel Sci. Technol. Int.* **1992**, *10* (3), 347−369.
(38) Al-Marzouqi, A. H.; Zekri, A. Y.; Azzam, A. A.; Dowaidar, A. *J. Porous Media* **2009**, *12* (6), 489−500.
(39) Okamoto, I.; Li, X.; Ohsumi, T. *Energy* **2005**, *30*, 2344−2351.
(40) Kharaka, Y. K.; Cole, D. R.; Hovorka, S. D.; Gunter, W. D.; Knauss, K. G.; Freifeld, B. M. *Geology* **2006**, *34* (7), 577−580.
(41) Alemu, B. L.; Aagaard, P.; Munz, I. A.; Skurtveit, E. *Appl. Geochem.* **2011**, *26*, 1975−1989.
(42) Liu, F.; Lu, P.; Griffith, C.; Hedges, S. W.; Soong, Y.; Hellevang, H.; Zhu, C. *Int. J. Greenhouse Gas Control* **2012**, *7*, 153−167.
(43) Roen, J. B. *Org. Geochem.* **1984**, *5* (4), 241−254.
(44) East, J. A.; Swezey, C. S; Repetski, J. E.; Hayba *Thermal maturity map of Devonian shale in the Illinois, Michigan, and Appalachian basins of North America*; Scientific Investigations Map 3214; U.S. Geological Survey: 2012.
(45) Peters, K. E. *AAPG Bull.* **1986**, *70* (3), 318−329.
(46) Espitalie, J.; Madec, M.; Tissot, B.; Mennig, J. J.; Leplat, P. Source Rock Characterization Method for Petroleum Exploration. Proceedings of the Offshore Technology Conference, Houston, Texas, May 2−5, 1977; OTC-2935-MS.
(47) Schumacher, B. A.; Shines, K. C.; Burton, J. V.; Papp, M. L.; Blume, L. J. *A comparison of soil sample homogenization techniques*; EPA 600/X-90/043; U.S. Environmental Protection Agency, Office of Research and Development: Las Vegas, NV, 1990.
(48) *Standard Test Method for Microscopical Determination of the Reflectance of Vitrinite Dispersed in Sedimentary Rocks*; ASTM Standard D7708; ASTM International: West Conshohocken, PA, 2011; DOI: 10.1520/D7708-11, www.astm.org.
(49) *Standard Practice for Preparing Coal Samples for Microscopical Analysis by Reflected Light*; ASTM Standard D2797; ASTM International: West Conshohocken, PA, 2011; DOI: 10.1520/D2797_D2797M-11A, www.astm.org.
(50) Pontolillo, J.; Stanton, R. W. *Coal petrographic laboratory procedures and safety manual II*; Open-File Report 94-631; U.S. Geological Survey: 1994.
(51) Biscaye, P. E. *Am. Mineral.* **1964**, *49*, 1281−1289.
(52) Hosterman, J. W.; Dulong, F. A computer program for semiquantitative mineral analysis of X-ray powder diffraction. In *CMS Workshop Lectures, Quantitative Mineral Analysis of Clays*; Pavear, D. R., Mumpton, F. A., Eds; The Clay Minerals Society: Evergreen, CO, 1989; Vol. *1*, pp 37−50.
(53) Burke, L. *Carbon dioxide fluid-flow modeling and injectivity calculations*; Scientific Investigations Report 2011-5083; U.S. Geological Survey: 2011.
(54) Bachu, S. *Environ. Geol.* **2003**, *44*, 277−289.
(55) Ouyang, L. *Open Pet. Eng. J.* **2011**, *5*, 13−21.
(56) Kolak, J. J. *A procedure for the supercritical fluid extraction of coal samples, with subsequent analysis of extracted hydrocarbons*; Open-File Report 2006-1054; U.S. Geological Survey: 2006.
(57) Peters, K. E.; Cassa, M. R. Applied Source Rock Geochemistry. In *Petroleum System—From Source to Trap*; Magoon, L. B., Dow, W. G., Eds.; AAPG Memoir 60; American Association of Petroleum Geologists: Tulsa, OK, 1994; pp 93−120.
(58) Ryder, R. T.; Hackley, P. C.; Alimi, H.; Trippi, M. H. *AAPG Search Discovery* **2013**, 10477.
(59) Repetski, J. E.; Ryder, R. T.; Weary, D. J.; Harris, A. G.; Trippi, M. H. *Thermal maturity patterns (CAI and %R_o) in Upper Ordovician and Devonian rocks of the Appalachian basin: A major revision of USGS Map I-917-E using new subsurface collections*; Scientific Investigations Map 3006; U.S. Geological Survey: 2008.
(60) Huc, A. Y.; Nederlof, P.; Debarre, R.; Carpentier, B.; Boussafir, M.; Laggoun-Défarge, F.; Lenail-Chouteau, A.; Bordas-Le Floch, N. *Chem. Geol.* **2000**, *168* (1), 99−112.
(61) Wilson, N. S. F. *Int. J. Coal Geol.* **2000**, *43*, 53−82.
(62) Bruner, K. R.; Smosna, R. *A comparative study of the Mississippian Barnet Shale, Fort Worth Basin, and Devonian Marcellus Shale, Appalachian Basin*; DOE/NETL-2011/1478; U.S. Department of Energy, National Energy Technology Laboratory: 2011.
(63) Hosterman, J. W.; Whitlow, S. I. *Clay mineralogy of Devonian shales in the Appalachian Basin*; Professional Paper 1298; U.S. Geological Survey: 1983.
(64) Laughrey, C. D.; Ruble, T. E.; Lemmens, H.; Kostelnik, J.; Butcher, A. R.; Walker, G.; Knowles, W. *AAPG Search Discovery* **2011**, 110150.
(65) Frysinger, G. S.; Gaines, R. B.; Xu, L.; Reddy, C. M. *Environ. Sci. Technol.* **2003**, *37*, 1653−1662.
(66) Ahmed, M.; George, S. C. *Org. Geochem.* **2004**, *35*, 137−155.
(67) Jarvie, D. M.; Baker, D. R. Application of the Rock-Eval III Oil Show Analyzer to the Study of Gaseous Hydrocarbons in an Oklahoma Gas Well. Presented at the Geochemistry Division, 187th ACS National Meeting, St. Louis, Missouri, April 8−13, 1984.
(68) Mullins, O. C.; Sabbah, H.; Eyssautier, J.; Pomerantz, A. E.; Barré, L.; Andrews, A. B.; Ruiz-Morales, Y.; Mostowfi, F.; McFarlane,

DOI: 10.1021/acs.energyfuels.5b02059
Energy Fuels 2015, 29, 7897−7909

R.; Goual, L.; Lepkowicz, R.; Cooper, T.; Orbulescu, J.; Leblanc, R. M.; Edwards, J.; Zare, R. N. *Energy Fuels* **2012**, *26* (7), 3986−4003.
(69) Sing, K. S. W.; Everett, D. H.; Haul, R. A. W.; Moscou, L.; Pierotti, R. A.; Rouquérol, J.; Siemieniewska, T. *Pure Appl. Chem.* **1985**, *57* (4), 603−619.
(70) Clarkson, C. R.; Freeman, M.; He, L.; Agamalian, M.; Melnichenko, Y. B.; Mastalerz, M.; Bustin, R. M.; Radlinski, A. P.; Blach, T. P. *Fuel* **2012**, *95*, 371−385.
(71) Larsen, J. W.; Hall, P.; Wernett, P. C. *Energy Fuels* **1995**, *9*, 324−330.
(72) Chalmers, G. R. L.; Bustin, R. M. *Int. J. Coal Geol.* **2007**, *70*, 223−239.
(73) Milliken, K. L.; Rudnicki, M.; Awwiller, D. N.; Zhang, T. *AAPG Bull.* **2013**, *97* (2), 177−200.
(74) Gu, X.; Cole, D. R.; Rother, G.; Mildner, D. F. R.; Brantley, S. L. *Energy Fuels* **2015**, *29*, 1295−1308.

DOI: 10.1021/acs.energyfuels.5b02059
Energy Fuels 2015, 29, 7897−7909